J|A|C|S
ARTICLES
Published on Web 10/11/2005

# Dependence of Field Switched Ordered Arrays of Dinuclear Mixed-Valence Complexes on the Distance between the Redox Centers and the Size of the Counterions

Hua Qi,[†] Anuradha Gupta,[†] Bruce C. Noll,[†] Gregory L. Snider,*[,‡] Yuhui Lu,[‡] Craig Lent,[‡] and Thomas P. Fehlner*[,†]

*Contribution from the Departments of Chemistry & Biochemistry, and Electrical Engineering, University of Notre Dame, Notre Dame, Indiana 46556*

Received July 7, 2005; E-mail: fehlner.1@nd.edu

***Abstract:*** *trans*-[$(H_2NCH_2CH_2C{\equiv}N)(dppe)_2Ru(C{\equiv}C)_6Ru(dppe)_2(N{\equiv}CCH_2CH_2NH_2)][PF_6]_2$, **2**$[PF_6]_2$, a derivative of *trans*-$[Cl(dppe)_2Ru(C{\equiv}C)_6Ru(dppe)_2Cl]$ functionalized for binding to a silicon substrate, has been prepared and characterized spectroscopically, electrochemically, and with a solid state, single-crystal structure determination. Covalent binding via reaction of one amine group to a boron-doped, smooth Si−Cl substrate is verified by XPS measurements and surface electrochemistry. Vertical orientation is demonstrated by film thickness measurements. Synthesis of the **2**$[PF_6]_3$ mixed-valence complex on the surface is established by electrochemical techniques. Measurement of the ac capacitance of the film at 1 MHz as a function of voltage across the film with a pulse−counter pulse technique demonstrates controlled electric field generation of the two stable mixed-valence forms differing in the spatial location of one electron, that is, switching. As compared to [*trans*-$Ru(dppm)_2(C{\equiv}CFc)(NCCH_2CH_2NH_2)][PF_6][Cl]$, **1**$[PF_6][Cl]$, the magnitude of the capacitance signal per complex observed on switching is shown to increase with increasing distance between the metal centers. Additional experiments on **1**[X][Cl] show that the potential for switching **1**[X][Cl] increases in the order $[X]^- = [SO_3CF_3]^- < [PF_6]^- < [Cl]^-$. A simple electrostatic model suggests that the smaller is the counterion, the greater is the perturbation of the metal sites and the larger is the barrier for switching.

## Introduction

Absorption of a photon by a dinuclear mixed-valence complex at the energy of the intervalence charge-transfer band moves an electron from one metal site to the other.[1] In a recent study, we demonstrated for the first time that one can accomplish the same electron transfer by the application of an external electric field to an oriented array of mixed-valence complexes.[2] The significance of this work lies in a proposed application for mixed-valence complexes in a nontransistor-based paradigm for molecular electronics. External electric field control of the position of an electron in a mixed-valence complex is a necessary property for this application.

Thus, the Quantum Cellular Automata (QCA) paradigm transmits binary information utilizing electric field coupled cells rather than current flow.[3−5] This method has been proven using cells constructed of quantum dots but only at very low temperatures as state energy differences of the cell configurations are low.[6] For molecular-sized components, state energy differences are large relative to thermal energy at room temperature. High level calculations verify that the fundamental principles of QCA apply on the molecular scale.[7,8] Empirical demonstration of these principles follows albeit at a slower pace.

Our experiments, which focus on electron transport within a single molecule, are related to the much studied problem of electron transport through molecules, an intrinsically harder problem due to difficulties in dealing with the required molecule−metal junctions.[9−12] Characterization and control of both inter- and intramolecular current flow is of significant fundamental interest even in the absence of applications to molecular electronics.

In our first work, the surface bound and oriented unsymmetrical mixed-valence complex [*trans*-$Ru(dppm)_2(C{\equiv}CFc)(NCCH_2CH_2NH_2)][PF_6]_2$, **1**$[PF_6]_2$, where dppm = methylbis(diphenylphosphane) and Fc = $(\eta^5\text{-}C_5H_5)Fe(\eta^5\text{-}C_5H_4)$, was used

[†] Department of Chemistry & Biochemistry.
[‡] Department of Electrical Engineering.

(1) Ward, M. D. *Chem. Soc. Rev.* **1995**, 121.
(2) Qi, H.; Sharma, S.; Li, Z.; Snider, G. L.; Orlov, A. O.; Lent, C. S.; Fehlner, T. P. *J. Am. Chem. Soc.* **2003**, *125*, 15250.
(3) Lent, C. S.; Tougaw, P. D.; Porod, W.; Bernstein, G. H. *Nanotechology* **1993**, *4*, 49.
(4) Lent, C. S. *Science* **2000**, *288*, 1597.
(5) Lent, C. S.; Lieberman, M. *Abstr. Papers, American Chemical Society, Fall Meeting*; American Chemical Society: Washington, DC, 2002; Vol. 035 COMP, p 224.
(6) Orlov, A. O.; Amlani, I.; Bernstein, G. H.; Lent, C. S.; Snider, G. L. *Science* **1997**, *277*, 928.
(7) Braun-Sand, S. B.; Wiest, O. *J. Phys. Chem. A* **2003**, *107*, 285.
(8) Lent, C. S.; Isakaen, B.; Lieberman, M. *J. Am. Chem. Soc.* **2003**, *125*, 1056.
(9) Kubatkin, S.; Danilov, A.; Hjort, M.; Cornil, J.; Bredas, J.-L.; Stuhr-Hansen, N.; Hedegard, P.; Bjornholm, T. *Nature* **2003**, *425*, 698.
(10) Damle, P.; Rakshit, T.; Paulsson, M.; Datta, S. *IEEE Trans. Nanotech.* **2002**, *1*, 145.
(11) Reed, M. A.; Zhou, C.; Muller, C. J.; Burgin, T. P.; Tour, J. M. *Science* **1997**, *278*, 252.
(12) Nazin, G. V.; Qiu, X. H.; Ho, W. *Science* **2003**, *302*, 77.


**10.1021/ja054508j CCC: $30.25** 

***Scheme 1.*** Schematic Representation of Oriented, Surface Bound Mixed-Valence Complexes in a Capacitor Structure with Parallel Hg and Doped Si Plates

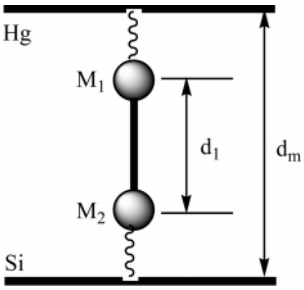


as a prototype of a biased two-dot molecular quantum cellular automata (QCA) cell with the electron occupying the ruthenium site in the absence of a perturbing field.[13] On application of an electric field of proper polarity along the metal−metal axis, the iron site is stabilized leading to electron transfer from ruthenium to iron and cell switching. Experimentally, the array of complexes between two electrodes (Scheme 1) generates an ac capacitance signal at the switching potential, which arises from the reorientation of the dipole caused by moving the electron between the two metals.

Although the earlier measurements established the viability of electric field driven switching of mixed-valence complexes,[2] it generated additional questions that need to be addressed. Three of these are: (a) the dependence of the intensity of the dipolar response to switching on *d* the distance between the metal centers (Scheme 1); (b) the consequences of removing the dissymmetry between metal centers; and (c) the effects of counterions on the switching potential. Point (a) addresses the ability to control the magnitude of the dipolar switching field, which ultimately will be used to switch adjacent cells in a QCA wire or device; (b) addresses the suitability of a delocalized mixed-valence complex for use as a QCA cell; and (c) addresses the sensitivity of the switching potential to the number and type of counterions.

As the device used to detect switching is a parallel plate capacitor, the charge associated with the capacitance signal observed on switching is given by the equation,[2] $Q/A\sigma_m = e(d/d_m)$, where $Q$ is the charge represented by the measured capacitance peak, $\sigma_m$ is the density of active cells on the surface, $e$ is the electron charge, $A$ is the area of the capacitor plates measured, $d$ is the distance the electron moves between two metal centers, and $d_m$ is the distance between the capacitor plates which equals the length of the molecule. Thus, the switching signal intensity per molecule depends on the ratio of $d/d_m$. If the change in $d$ dominates any change in the size of the ligand envelopes at the metal centers, then the signal intensity should be enhanced as the conjugated linker between the metal centers is lengthened. Hence, objective (a) can be explored by increasing the number of carbyne units in the alkyne linker between the metal centers.

A symmetrical Robin/Day Type III mixed-valence complex with a ground-state delocalized between the two redox centers[14,15] may be considered unusable for molecular QCA, as it does not possess the binary states necessary to encode information. On the other hand, the perturbation caused by surface binding, the spatial location of counterions, or the applied electric field itself may be sufficient to localize the electron. Taking a totally pragmatic approach, the successful demonstration of switching of a symmetrical mixed valence with a delocalized ground state in the manner of **1**$[PF_6]_2$ would settle question (b) one way or the other.

Point (c) arises from the fact that two different switching potentials were observed in arrays formed from **1**$[PF_6]$.[2] These were associated with different cation−anion combinations on the surface based on correlation of relative signal intensities with relative anion surface concentrations. As the difference in switching potentials is large, the influence of the counterions is correspondingly large. Hence, this point has been revisited to further define the role of the counterions.

The new studies have been designed to allow to utilization of the same set of chemical and surface techniques demonstrably useful in the earlier study. Thus, one of the metal centers, the conjugated linker type, the surface linker and binding chemistry, the characterization techniques, and the capacitance measuring technique are the same in this work as in the earlier study.

A molecule with the necessary attributes is derived from the known symmetrical complex *trans*-$[Cl(dppe)_2Ru(C{\equiv}C)_6Ru(dppe)_2Cl]$, dppe = diphenylphosphinoethane, which contains a rigid 12 carbon atom linker between the metal centers.[16] The Cl ligands trans to the poliyne bridge provide a chemical handle for attachment of the short $NCCH_2CH_2NH_2$ surface linker used previously. Reaction of the amine with a chlorinated Si surface generates a covalently bound complex.[17,18] The functionalized precursor to the mixed-valence complex, *trans*-$[(H_2NCH_2CH_2C{\equiv}N)(dppe)_2Ru(C{\equiv}C)_6Ru(dppe)_2(N{\equiv}CCH_2CH_2NH_2)][PF_6]_2$, **2**$[PF_6]_2$, retains a symmetrical structure in solution. Once bound to a Si surface, it is no longer symmetrical, albeit the extent of the electronic perturbation is not known a priori. Finally, a mixed-valence complex can be generated by oxidation to the trication. Quantum chemical calculations can be used to judge the extent of delocalization of the ground state of $\mathbf{2}^{3+}$.

## Results and Discussion

**Synthesis and Structure.** Following literature procedures,[16,19] the synthesis of the dinuclear complex, *trans*-$[Cl(dppe)_2Ru(C{\equiv}C)_6Ru(dppe)_2Cl]$, dppe = diphenylphosphinoethane, was carried out. We, too, failed to obtain crystals suitable for a definitive structure determination, and formation of the desired product was confirmed by the measured spectroscopic data. The procedure used successfully in the functionalization of **1**$[PF_6]$[13] led to low yields of **2**$[PF_6]_2$ and contamination with mononuclear side products, for example, *trans*-$[(H_2NCH_2CH_2C{\equiv}N)(dppe)_2Ru{-}Cl][PF_6]$. However, changing solvents from $CH_2Cl_2$ to toluene, attention to the purity of the dichloro-complex, and stoichiometric addition of a stock solution of the reagent resulted in satisfactory yields (>50%) of the desired functionalized molecule (Scheme 2).

The $^1$H NMR of **2**$[PF_6]_2$ shows two triplets at $\delta$ 2.37 and 1.83, which are assigned to the $CH_2$ groups of the amine linker.

(13) Li, Z.; Beatty, A. M.; Fehlner, T. P. *Inorg. Chem.* **2003**, *42*, 5707.
(14) Robin, M. B.; Day, P. *Adv. Inorg. Chem. Radiochem.* **1967**, *10*, 247.
(15) Demadis, K. D.; Hartshorn, C. M.; Meyer, T. J. *Chem. Rev.* **2001**, *101*, 2655.
(16) Rigaut, S.; Perruchon, J.; Le Pichon, L.; Touchard, D.; Dixneuf, P. H. *J. Organomet. Chem.* **2003**, *670*, 37.
(17) Bergerson, W. F.; Mulder, J. A.; Hsung, R. P.; Zhu, X.-Y. *J. Am. Chem. Soc.* **1999**, *121*, 454.
(18) Zhu, X.-Y.; Mulder, J. A.; Bergerson, W. F. *Langmuir* **1999**, *15*, 8147.
(19) Chaudret, B.; Commenges, G.; Poilblanc, R. J. *J. Chem. Soc., Dalton Trans.* **1984**, 1635.

***Scheme 2.*** Functionalization of *trans*-[Cl(dppe)$_2$Ru(C≡C)$_6$Ru(dppe)$_2$Cl] for Surface Binding

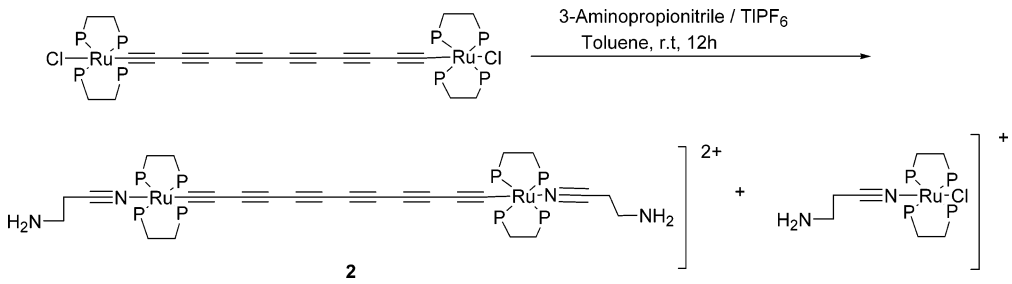


**2**

The increased shielding of these protons relative to the free linker molecule, although not as large as observed for **1**[$PF_6$][13] with dppm ligands, is also attributed to ring current effects of the phenyl groups, which form a pocket containing the ethylene moiety of the linker. Thus, the shift confirms successful coordination of the linker to Ru. The six $^{13}$C NMR resonances between $\delta$ 127−52 are characteristic of the six unique carbon atoms of the poliyne chain between the ruthenium atoms.[20] The remaining multinuclear NMR data and IR data corroborate linker attachment without disruption of the poliyne bridge between the metal centers.

Unambiguous characterization resulted from the fact that addition of the surface linkers generates a salt that forms single crystals suitable for an X-ray diffraction study. The structure of **2**[$PF_6$]$_2$ in the solid state is shown in Figure 1 and fully confirms the structure based on the solution data. Pertinent to this study is the distance between two ruthenium centers in Ru−(C≡C)$_6$−Ru of 17.70 Å, which is comparable to that between the iron atoms in Fp*(C≡C)$_6$Fp*.[21] Note that the poliyne bridge is bent but its nonlinearity of 37.4°/6.2° (measured as the sum and average deviation of the C−C−C bond angles from 180°) is comparable to that of 57.5°/4.8° for Fp*(C≡C)$_6$Fp*. Alternating long and short bond distances (av 1.19 and 1.36 Å) are observed in **2**[$PF_6$]$_2$, confirming the poliyne, C≡C−C, formulation. The other parameters associated with the Ru center are comparable to those found in **1**[$PF_6$],[4] bearing in mind the differences between dppm and dppe ligands.

The neutral dichloro precursor of **2**[$PF_6$]$_2$ exhibits two successive, reversible oxidation waves corresponding to the formation of the mixed-valence monocation and the dication, and the 230 mV splitting between the two waves reflects a comproportionation constant of $10^4$ sufficient for our purposes.[16] The first oxidation of **2**[$PF_6$]$_2$ (Figure 2) occurs about 0.2 V more positive than its neutral precursor, which is approximately the same shift observed in going from *trans*-ClRu(dppm)$_2$(C≡CFc) to **1**[$PF_6$] in the same solvent.[13] As was also found before, the substitution of [Cl]$^-$ by $NCCH_2CH_2NH_2$ results in an irreversible second oxidation. Scanning to higher positive potentials and repetitive scanning showed evidence of degradation in solution.

**Nature of Mixed-Valence $2^{3+}$.** To characterize the ground state of mixed-valence $2^{3+}$, quantum chemical calculations were carried out on a model compound, designated $2^{3+}$(H), in which all of the phenyl substituents are replaced by hydrogen atoms. This simplification allows high-quality calculations from which the essential aspects of the molecular charge configurations can be determined.

The optimized structure of $2^{3+}$**(H)** demonstrates a zero dipole moment. Figure 3a gives the electrostatic potential surface of $2^{3+}$**(H)** and suggests the positive charge is distributed uniformly between the two metal centers. A detailed Mulliken charge analysis shows that each redox center may be assigned a charge of 1.5. Figure 3b shows the highest occupied molecular orbital (HOMO) from which we can see that the odd electron is delocalized over the two Ru moieties. Hence, the molecule can be viewed as a Robin−Day Type III mixed-valence complex.[14] For comparison, discussion of other Type III $Ru^{II}$−$Ru^{III}$ systems may be found in the literature.[15,22]

To test whether an external field can cause localization, the electronic structure of $2^{3+}$**(H)** is investigated under a uniform field applied between the two redox centers. The results show that the dipole moment of $2^{3+}$**(H)** increases as the external field strengthens. When the amplitude of the electric field reaches 1 V/nm, the dipole moment is 8.4 e Å, which is reasonable considering the distance between the two Ru atoms is more than 10 Å. The Mulliken charge distribution reveals a charge of +1.1 at one end and +1.9 at the other. The electrostatic potential in Figure 4a shows that one redox center is more highly charged than the other under the influence of the applied field. The

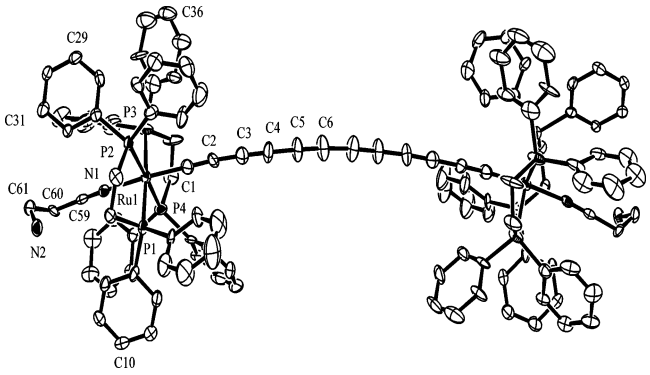


***Figure 1.*** Molecular structure of *trans*-[(H$_2$NCH$_2$CH$_2$C≡N)(dppe)$_2$Ru(C≡C)$_6$Ru(dppe)$_2$(N≡CCH$_2$CH$_2$NH$_2$)][$PF_6$]$_2$, **2**[$PF_6$]$_2$. The [$PF_6$]$^-$ anions are not shown.

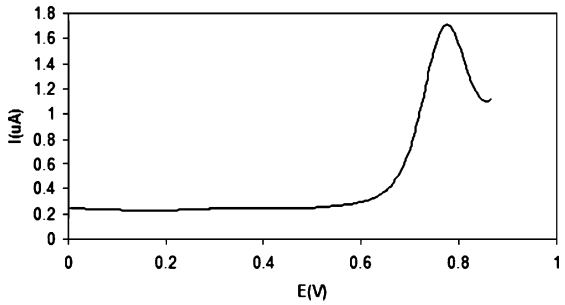


***Figure 2.*** Square wave voltammogram of **2**[$PF_6$]$_2$ in solution (100 mV/s, 0.1 M TBAP$F_6$ in $CH_2Cl_2$, Pt wire pseudo reference electrode).

(20) Dembinski, R.; Bartik, T.; Bartik, B.; Jaeger, M.; Gladysz, J. A. *J. Am. Chem. Soc.* **2000**, *122*, 810.
(21) Sakurai, A.; Akita, M.; Moro-oka, Y. *Organometallics* **1999**, *18*, 3241.

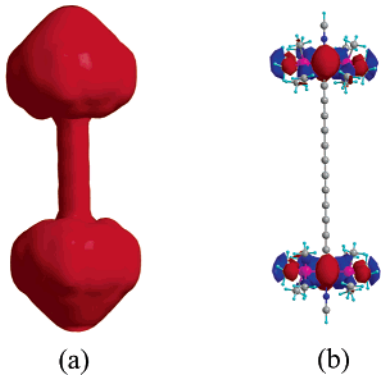


***Figure 3.*** (a) Electrostatic potential surface and (b) charge distribution in the HOMO for $\mathbf{2}^{3+}$**(H)**.

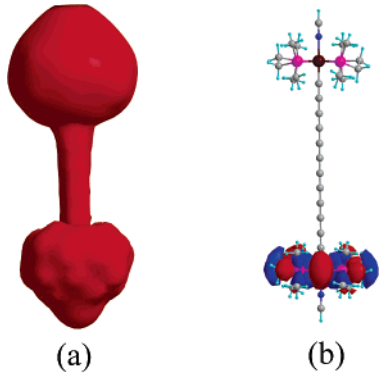


***Figure 4.*** (a) Electrostatic potential surface and (b) charge distribution in the HOMO for $\mathbf{2}^{3+}$**(H)** in a uniform electric field of 1 V/nm.

HOMO orbital pictured in Figure 4b also demonstrates that the odd electron is localized on one Ru moiety. These results suggest that, although $\mathbf{2}^{3+}$**(H)** is a totally delocalized Class III mixed-valence molecule, it is still suitable for QCA use. This will be true as long as the field of the adjacent molecule is sufficient to break the symmetry of the two quantum wells so that the odd electron localizes in the well of lower energy.

**Surface Attachment.** The complex **2**$[PF_6]_2$ has the same surface binding linker used with **1**$[PF_6]$ in the previous study. Hence, the same surface reaction chemistry was used to covalently bind and orient **2**$[PF_6]_2$ on a boron-doped Si(111) substrate as illustrated in Figure 5. Briefly, a clean, smooth Si (111) substrate with a thin oxide film is converted to a hydrogen-terminated surface with HF. Reaction with chlorine gas generates a chlorinated silicon surface suitable for reaction with the amine group of the linker to form the surface bound complex.[2,17,18]

The solvent $CH_2Cl_2$ used for **1**$[PF_6]$ was unsatisfactory because the low solubility of **2**$[PF_6]$ leads to slow attachment accompanied by degradation of **2**$[PF_6]_2$. Acetonitrile provides sufficient solubility to permit the same concentration of **2**$[PF_6]_2$ ($\sim$1 mM) as that used with **1**$[PF_6]$. Still, even though **2**$[PF_6]_2$ possesses two reactive amine groups, only 15% coverage of 2$[PF_6]_2$ is achieved in 72 h. In contrast, coverage of **1**$[PF_6]$ saturates at 45% at 30 h. Note that the poliyne chain between the two metal centers in **2**$[PF_6]_2$ does not allow more than one amine group to react with the silicon substrate. Because of the greater air sensitivity of **2**$[PF_6]_2$ versus **1**$[PF_6]$, the entire surface preparation was performed in a drybox. After preparation, the films were lightly washed with organic solvents but not water. The Si surface preparation and molecule tethering reaction were monitored by X-ray photoelectron spectroscopy (XPS).

**Film Characterization.** Composition data on the silicon bound films of **2**$[PF_6]_2$ were obtained by XPS. Representative spectra are shown in Figure 6, and a table of binding energies will be found in the Supporting Information. XPS analysis of a clean silicon substrate showed no measurable levels of the elements used to define the presence of **2**$[PF_6]_2$. Films of **2**$[PF_6]_2$ show the characteristic spin−orbit split Ru 3p ionizations at 484 and 462 eV as well as ionizations characteristic of N, P, C, F (counterion), Cl (un-reacted Cl), Si (substrate), B (dopant), and O (impurity).

In the earlier work, the vigorous methods used to ensure removal of any physically bound **1**$[PF_6]$ created an unexpected complication as most or all of the $[PF_6]^-$ counterions were lost. This was evidenced by low intensity or no F signal in the XPS of films of **1**$[PF_6]$ prepared in this manner. Given the more fragile character of **2**$[PF_6]_2$, the films of this compound were treated more gently, that is, no sonication or water. Retention of the $[PF_6]^-$ counterions is reflected by the strong F signal (Figure 6). Using the raw area and standard sensitivity factors, the ratio of F versus Ru in XPS of **2**$[PF_6]_2$ films is 2.7:1 versus 6:1 theoretical. Considering the poor S/N for Ru, the XPS data suggest that most of the $[PF_6]^-$ is retained. In this work, rather than exhaustive washing, we relied on the surface electrochemical data to confirm strong bonding of the complex to the surface.[23]

A perpendicular orientation of the bound **2**$[PF_6]_2$ complexes relative to the plane of the Si surface is required to observe switching. Because variable angle XPS is not an option for this symmetrical complex, film thickness was used as an experimental indicator of orientation. An average of 10 ellipsometric measurements yields a mean film thickness of 27.7 $\pm$ 0.8 Å, which is closer to the long dimension of **2**$[PF_6]_2$ (28 Å), derived from the X-ray diffraction study, than its width (13 Å). This conclusion is corroborated by an analysis of the N 1s peak, which is significantly broader that that observed for **1**$[PF_6]$. The data, curve resolution, and analysis may be found in the Supporting Information where it is shown that the difference in intensity of the two N peaks suggests one N atom is 26 Å above the position of the other in the film. Hence, it supports a near vertical orientation.

Why should the bound complex have a predominantly perpendicular arrangement? We showed that for **1**$[PF_6]$, the size of the phenyl groups of the dppm ligands on Ru combined with the short surface linker enforces a vertical orientation, which was experimentally verified by variable angle XPS. The surface binding ends of **1**$[PF_6]$ and **2**$[PF_6]_2$ are similar as dppm and dppe ligands differ only by the presence of one versus two $CH_2$ groups in the diphosphine backbone. Thus, as illustrated by the simulation of **2**$[PF_6]_2$ bound to an ideal Si(111) surface in Figure 7, the phenyl groups of the dppe ligands of **2**$[PF_6]_2$ also support perpendicular orientation. Flexing of the poliyne linker between the metals and surface irregularities will result in a distribution of angles, thereby reducing the perpendicular component of the overall dipole and the overall intensity of the switching signal.

(22) Bencini, A.; Ciofini, I.; Daul, C. A.; Ferretti, A. *J. Am. Chem. Soc.* **1999**, *121*, 11418.

(23) Bard, A. J.; Faulkner, L. R. *Electrochemical Methods*; Wiley: New York, 2001.

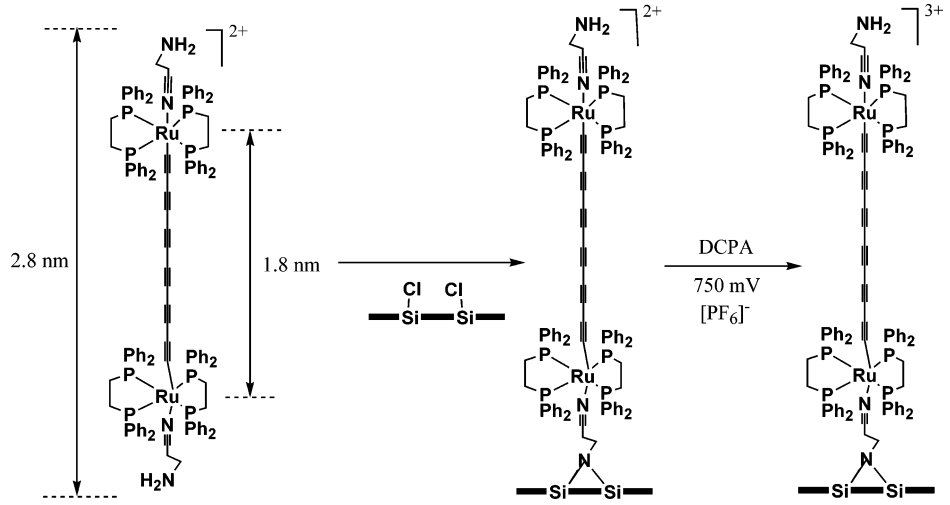


***Figure 5.*** Reaction of **2**$[PF_6]_2$ with a chlorinated Si(111) surface to generate surface bound **2**$[PF_6]_2$ with subsequent electrochemical oxidation to generate the surface bound, vertical mixed-valence complex.

Binding and vertical orientation of **2**$[PF_6]_2$ has been demonstrated; however, the molecules must retain redox activity as well. Surface electrochemical techniques not only confirm redox activity but also demonstrate strong surface binding. As shown in Figure 8, square wave voltametry of films of **2**$[PF_6]_2$ on boron-doped substrate give reversible peaks (143 mV fwhm, $\Delta$(anodic−cathodic) = 30 mV): for context, ideal, noninteracting, strongly bound redox centers exhibit 91 mV fwhm, $\Delta$(anodic−cathodic) = 0 mV; and films formed from **1**$[PF_6]$ show 140 mV fwhm, $\Delta$(anodic−cathodic) = 40 mV.[23−25]

The electrochemical measurements also provide an important parameter, the surface coverage of redox active complexes. The area of the square wave curves in Figure 8 represents a total charge of $6.6 \times 10^{-6}$ C required to oxidize the film. When combined with the electrode surface area of 3.5 $cm^2$ and an estimated cross-sectional area of $1.3 \times 10^{-14}$ $cm^2$ per molecule, the areal density of redox sites calculated is $1.6 \times 10^{13}$ $cm^{-2}$ (15% coverage).

Oxidation of **1**$[PF_6]$ was successfully demonstrated with both ferrocenium ion as well as fixed potential electrolysis. Electrolysis gives a better yield of mixed-valence complexes on the surface. The higher oxidation potential required for **2**$[PF_6]_2$ made electrolysis the method of choice to generate the required mixed-valence ion, **2**$[PF_6]_3$, on the surface. Based on the square wave voltametry, an oxidizing potential of 750 mV was applied in a supporting electrolyte of tetrabutylammonium hexafluorophosphate [TBA]$[PF_6]$ in $CH_3CN$. As these films were not as robust as films of **1**$[PF_6]$, a dc potential amperometric (DCPA) procedure was used to determine the net yield of mixed-valence complexes generated in the film as a function of oxidizing time. The analytical probe is a −100 mV reducing potential applied immediately after the oxidation. The area under the exponentially decaying signal is a measure of the mixed-valence complex.

As illustrated in Figure 9, analysis immediately after the film is oxidized shows 11% of the oxidized molecules have survived a 2 s oxidation. Oxidation for 10 s results in a 5% yield of oxidized molecules, and 60 s completely destroys the electrochemical activity of the film; that is, the number of surviving electrochemically active **2**$[PF_6]_2$ complexes on the surface depends strongly on the oxidation time. A 2 s oxidation time at 750 mV was adopted for use. Note that, although the film had a short lifetime under the applied oxidizing potential in the electrochemical cell, once oxidized the dry films survived for hours out of solution. The dry, unoxidized films retain electrochemical activity after storage over a month in a drybox.

**Capacitance Measurements.** To provide a baseline measurement, a single wafer with a film of **2**$[PF_6]_2$ is divided into two pieces. One part is oxidized electrochemically and stored along with the unoxidized control sample under inert gas. Although the capacitance measurements on the dry films were carried out in air, the signals observed (see below) did not change significantly for up to 2 h in the air. Figure 10 shows the ac capacitance of a film as a function of applied potential between the Hg electrodes for films of **2**$[PF_6]_2$ and **2**$[PF_6]_3$. It is important to remember that any reversible redox activity, for example, between the Si or Hg plates of the capacitor, which gives rise to spurious capacitance changes, will be observed in both the unoxidized control sample and the oxidized sample. Hence, the difference between the two measurements identifies capacitance changes solely associated with the mixed-valence complex. The switching potential of the mixed-valence complex **2**$[PF_6]_3$ is −0.2 V on the central Hg spot relative to the annular Hg electrode.

Measurements at six different surface positions are internally consistent, and two representative measurements are shown in Figure 10. The capacitance peak generated at the switching potential represents an average charge of $6.9 \times 10^{-11}$ C (seven measurements) from which a $\sigma_m = 1.3 \times 10^{11}$ $cm^{-2}$ ($d = 1.8$ nm, $d_m = 2.8$ nm, $A = 5 \times 10^{-3}$ $cm^2$) may be calculated. The surface density of **2**$[PF_6]_2$ from the surface electrochemical measurements is $1.6 \times 10^{13}$ $cm^{-2}$, and the density of mixed-valence **2**$[PF_6]_3$ from the DCPA results is $1.8 \times 10^{12}$ $cm^{-2}$. As found for **1**$[PF_6]_2$, the surface density calculated from the switching signal is an order of magnitude lower than that obtained electrochemically.

**The Switching Characteristics of 2$[PF_6]_3$ versus 1$[X]_2$, Where X = $PF_6$ or Cl.** The first two points, (a) and (b), raised in the Introduction may now be addressed. The dependence of

(24) Li, Z.; Fehlner, T. P. *Inorg. Chem.* **2003**, *42*, 5715.
(25) Auletta, T.; van Veggel, F. C. J. M.; Reinhoudt, D. N. *Langmuir* **2002**, *18*, 1288.

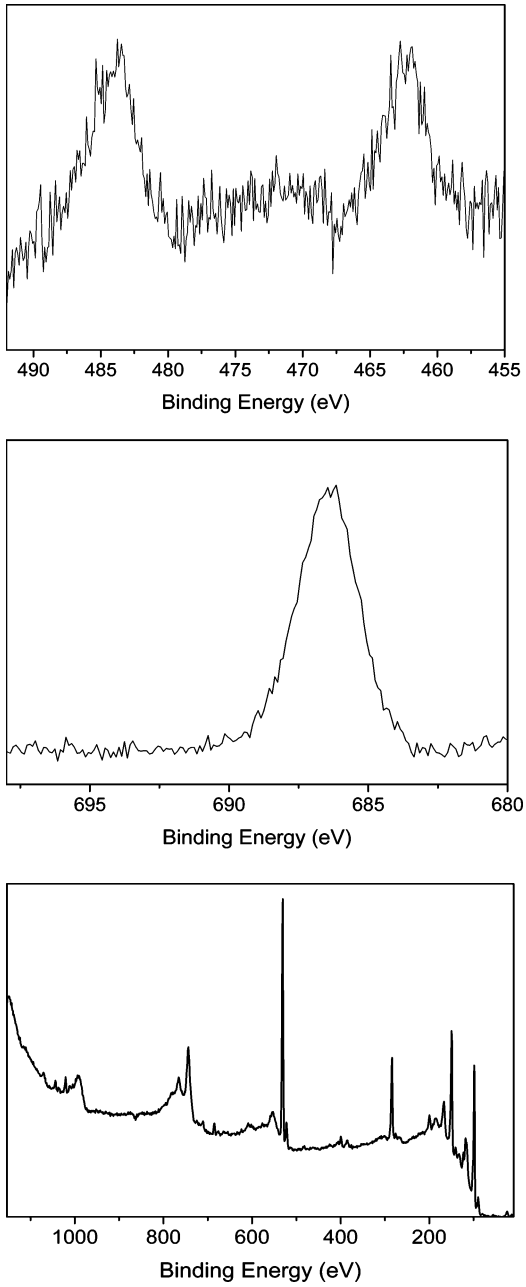


***Figure 6.*** Selected XPS spectra of **2**$[PF_6]_2$ bound to a boron-doped Si(111) surface. Top, Ru 3p; center, F 1s; bottom, survey spectrum.

signal intensity on distance between the redox centers is straightforward and can be illustrated by a variation of the calculation given just above. That is, a plot of $Q/(\sigma_m A)$ versus $d/d_m$ should be linear with a slope equal to the charge on the electron. Using $Q_1 = 4.1 \times 10^{-11}$ C (15 measurements), $\sigma_{m1} = 4 \times 10^{12}$ cm$^{-2}$, $A_1 = 2 \times 10^{-3}$ cm$^2$, $(d/d_m)_1 = 0.6/1.8$ for **1**$[X]_2$ from the earlier work and $Q_2 = 6.9 \times 10^{-11}$ C, $\sigma_{m2} = 1.8 \times 10^{12}$ cm$^{-2}$, $A_2 = 5 \times 10^{-3}$ cm$^2$, $(d/d_m)_2 = 1.8/2.8$ for **2**$[PF_6]_3$ from the present work, the two data points shown in Figure 11 are obtained. The slope is $8 \times 10^{-20}$ C as compared to the accepted value of $1.6 \times 10^{-19}$ C for the charge on the electron. Considering the uncertainties in the measurements, quantitative agreement is not expected. Still, it is clear that the dipolar response increases as the distance between metal centers increases. This means that the dipolar field generated by a two-dot molecular QCA cell can be varied by adjusting the length

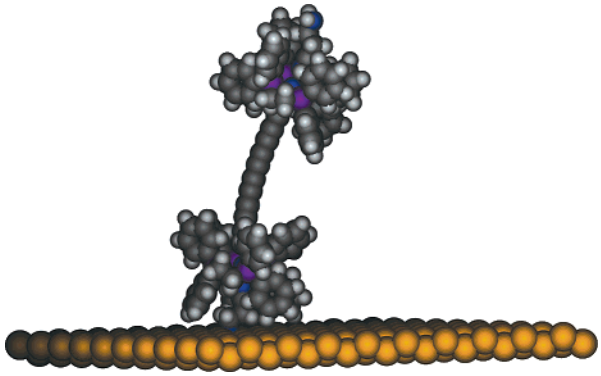

***Figure 7.*** Space-filling model of docking of **2**$[PF_6]_2$ to a Si(111) surface ($d_{N-Si} = 2.1$ Å, $-Si-N-Si = 135°$) showing the near vertical orientation supported by the phenyl groups of the dppe ligands. The counterions are not shown.

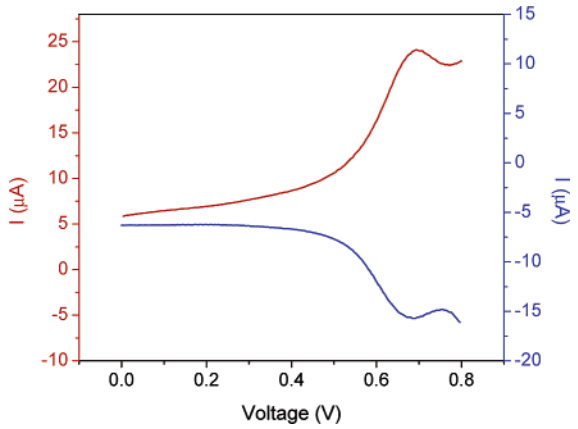


***Figure 8.*** Square wave voltametry of **2**$[PF_6]_2$ on a Si(111) surface (100 mV/s, 0.1 M [TBA][$PF_6$] in $CH_3CN$; red, forward scan; blue, reverse scan).

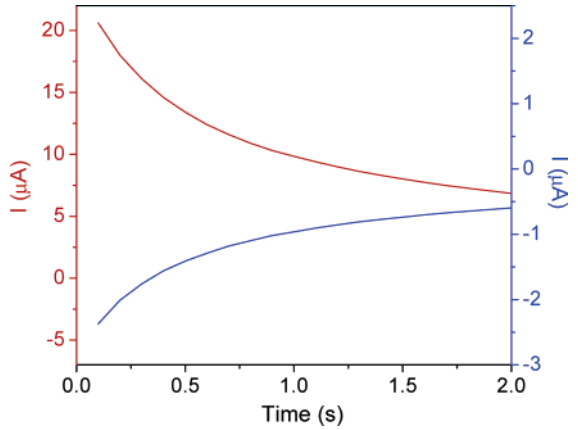


***Figure 9.*** DCPA oxidation of a film of **2**$[PF_6]_2$ on silicon at 750 mV (red) and subsequent reduction of the same film at −100 mV (blue) showing an overall yield of 11%.

of the conjugated metal linker in the mixed-valence complex. In a QCA device, it is just this field that couples adjacent cells and serves to transmit binary information from one cell to the next. In a molecular QCA cell, where the bulk of the ancillary ligands limit the closest approach of adjacent cells, the capability of adjusting the field strength coupling cells is a significant advantage.

The differences between symmetrical and unsymmetrical cells (point, (b)) are not so precisely addressed. What is clear is that symmetrical **2**$[PF_6]_3$ undergoes switching in the same manner

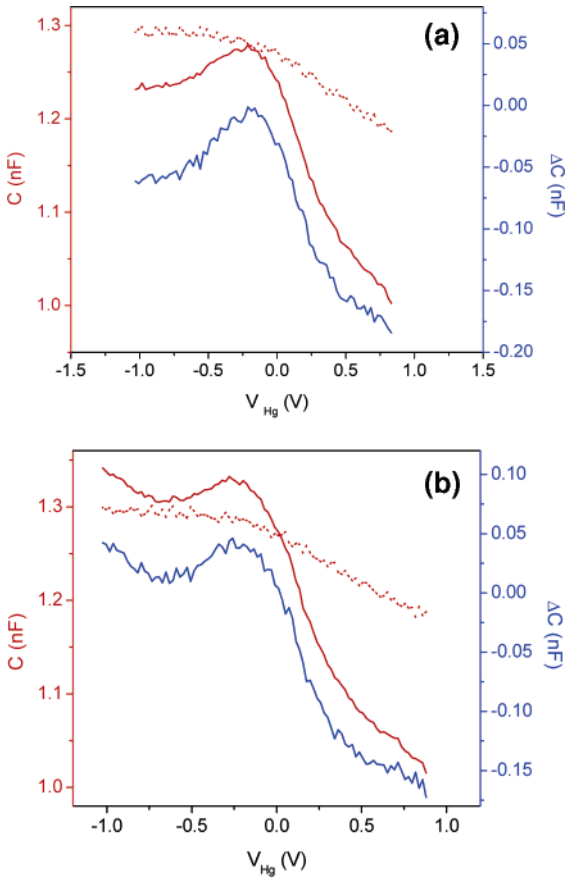


***Figure 10.*** Pulse/counterpulse ac capacitance measurements (4 ms on, 800 ms off) of the mixed-valence film of **2**$[PF_6]_3$ (solid red line), the control film of **2**$[PF_6]_2$ (dotted red line), and the difference (blue line) as a function of voltage.

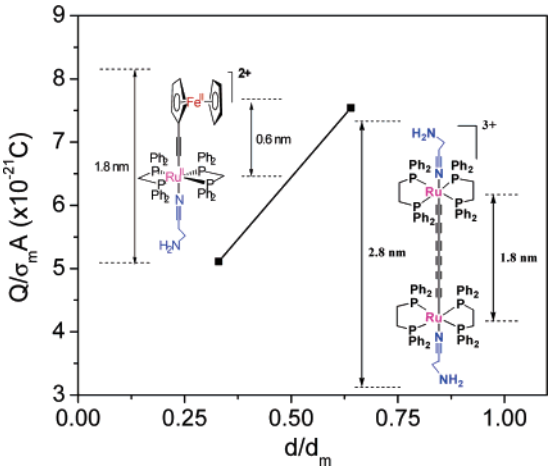


***Figure 11.*** A plot of $Q/(\sigma_m A)$ versus $d/d_m$ for **1**$[X]_2$, where X = $PF_6$ or Cl, and **2**$[PF_6]_3$ using the measured switching signals and the surface density of mixed-valence complexes from electrochemistry.

as the unsymmetrical complex. Either the perturbation caused by surface binding, the counterions, or the applied potential is sufficient to localize the mobile electron at one metal or the other independently of the nature of the free mixed-valence complex in solution. Hence, the distinction between Type II and Type III mixed-valence complexes in solution is not important when seeking systems for QCA applications.

Counterion effects, point (c), clearly dominate the switching behavior, as the difference in the two switching potentials for

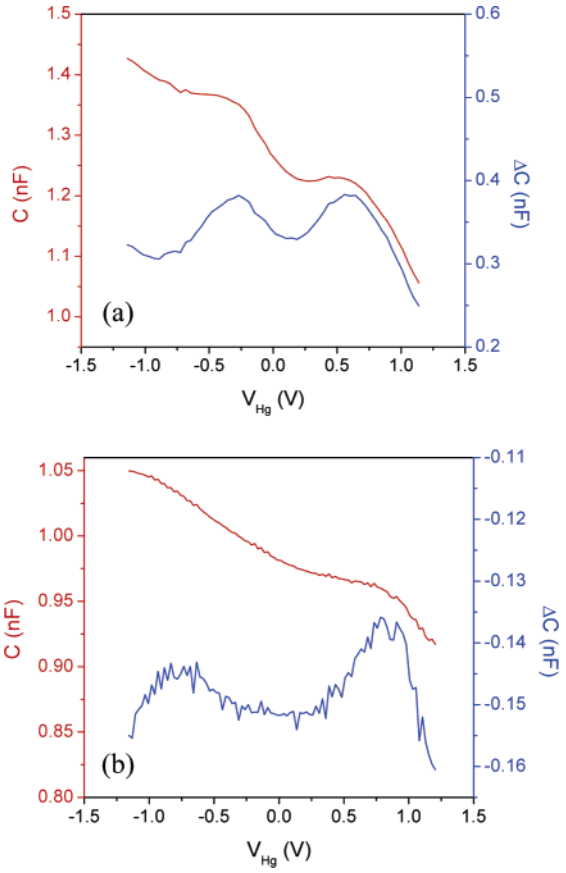


***Figure 12.*** (a) The switching potentials of **1**$[PF_6][Cl]$ and **1**$[Cl]_2$ using [FcH][$PF_6$] as oxidant and (b) the switching potentials **1**$[SO_3CF_3][Cl]$ and **1**$[Cl]_2$ using [FcH][$SO_3CF_3$] as oxidant. Red: mixed-valence film. Blue: mixed-valence film minus control film.

the **1**$[PF_6]$ system is 1 V. To investigate counterion effects further, we have carried out additional experiments on **1**$[PF_6]$ as it is a more robust complex than **2**$[PF_6]_2$. To review the earlier findings, binding of **1**$[PF_6]$ on the silicon substrate results in the loss of the counterion and formation of **1**[X], where [X] refers to a counterion other than $[PF_6]^-$. Based on the XPS analytical data, the only two logical possibilities are substrate $[Si-O]^-$ or $[Cl]^-$. Previously, we preferred the former, but the latter is also likely as hydrolysis of the excess Si−Cl bonds after binding of the complex generates $[Cl]^-$, which is never completely removed even with sonication. Stronger binding of the smaller anion may well drive the loss of $[PF_6]^-$ on repeated washing.

Oxidation with a ferrocenium $[PF_6]^-$ salt generated **1**$[PF_6][X]$, and two switching potentials were observed (Figure 12a). The one at −0.3 V was assigned to **1**$[PF_6][X]$, and that at 0.7 V was assigned to **1**$[X]_2$. Exhaustive washing of the film after oxidation lowered the $[PF_6]^-$ surface concentration and reduced the intensity of the switching peak at −0.3 V. These observations were independent of the method of oxidation (electrochemical vs chemical) and reproducible.

So what is $[X]^-$? Without repeating the earlier arguments, one not considered previously appears conclusive. If $[X]^-$ is $[Si-O]^-$, then the anion will be located in the silicon substrate much closer to the Ru site than the Fe site. If $[X]^-$ is $[Cl]^-$, then the anion will be located somewhere in the film but probably between the Fe and Ru sites where the shape of the ancillary ligand envelope permits. Recall the resting state has

the electron on Ru and the hole on Fe. Hence, it seems impossible that a surface $[Si-O]^-$ counterion requires a more positive switching potential than a $[PF_6]^-$ within the film. Simple electrostatic arguments suggest it should be the other way around. $[Cl]^-$ is the only other possibility for $[X]^-$. This leaves us with the problem of explaining why it is much easier to switch **1**$[PF_6][Cl]$ than 1$[Cl]_2$: hence, the new experiments on **1**$[PF_6]$.

The chemical oxidizing agent [ferrocenium]$[PF_6]$ used to oxidize films of **1**[Cl] was replaced by [ferrocenium]$[SO_3CF_3]$ to generate **1**$[SO_3CF_3][X]$ and **1**$[X]_2$. As shown in Figure 12b, switching at two potentials is again observed; however, one is at $-0.8$ V, and the other is at 0.8 V. The former is assigned to **1**$[SO_3CF_3][X]$ and lies 0.5 V more negative than **1**$[PF_6][Cl]$. Within experimental error, the latter is at the same potential as found for **1**$[Cl]_2$. These new results are consistent with the arguments above.

As three switching potentials for the same complex with different counterions have been measured, the origin of the large counterion effect can be explored further. First, realize that the zero of applied potential between the small area central Hg electrode and the large area annular Hg electrode is not the zero of potential across the film. The nominal voltage applied between these two electrodes must be corrected for the different work functions of Hg and p-doped Si. The first is 4.49 eV, whereas the latter may be estimated as the electron affinity of Si, which is the difference between the vacuum and conduction band (4.05 eV), plus the band gap for p-doped silicon (1.12 eV). The difference is $4.49-5.17 = -0.68$ eV, which suggests the actual zero of potential applied across the film is approximately $-0.7$ V. This correction would make the switching potentials: $[SO_3CF_3]^- = -0.1$ V; $[PF_6]^- = 0.4$ V; $[Cl]^- = 1.4$ V. Independently of the true zero of potential, the potential for switching **1**[Y][Cl] increases positively in the order $[Y]^- = [SO_3CF_3]^- < [PF_6]^- < [Cl]^-$.

This being the case, one can seek a correlation between counterion properties and switching potential. In the solvent-free environment of the film, the mobile counterions will position themselves relative to the surface bound mixed-valence cations to minimize charge separation, that is, form tight ion pairs, and one expects that the smaller is the negative ion, the tighter is the ion pair. The parameters of the measurements (1 MHz frequency of capacitance measurement, millisecond duration of applied potential, pulse-counter pulse mode to give an average applied potential of zero, relatively long resting time between pulse pairs) preclude significant ion movement; hence, the model shown in Figure 13 can be used to estimate the additional energy barrier caused by charge separation in moving the positive hole from Fe to Ru in the point charge field of the anion. The difference in the Coulombic energy between $Fe^{III}Ru^{II}$ (a) and $Fe^{II}Ru^{III}$ (b) is given by:

$$\Delta E = \text{const}\{1/(r_{Fe} + r) - 1/(r_{Ru} + r)\} = \text{const}(r_{Ru} - r_{Fe})\{1/(r_{Fe} + r)(r_{Ru} + r)\}$$

where $r_M$ is the radium of metal M and $r$ is the radius of the ion $[X]^-$.

Using standard covalent and van der Waals radii, the values for spherical $[Cl]^-$ and near spherical $[PF_6]^-$ are 0.175 and 0.325 nm, respectively. The approximate volume of nonspherical

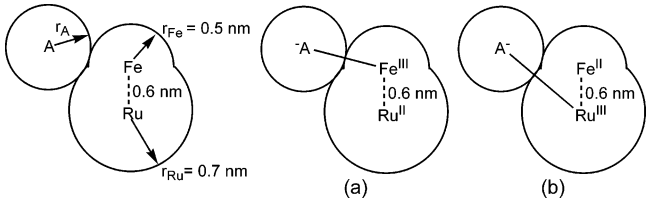


***Figure 13.*** Model of the anion−cation interactions for (a) resting state and (b) switched state.

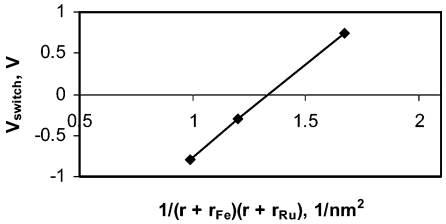


***Figure 14.*** Plot of $V_{switching}$ versus $1/(r + r_{Fe})(r + r_{Ru})$.

$[SO_3CF_3]^-$ is estimated as 2 times that of $[PF_6]^-$; hence, a value of $r$ that scales as the volume of a spherical ion is used, that is, 1.26 (0.325 nm) = 4.09 nm. A plot of $V_{switching}$ versus $1/(r_{Fe} + r)(r_{Ru} + r)$ in Figure 14 shows a good correlation with the size of the counterion. We suggest, then, that the major effect of the counterion is perturbation of the potential at which the energy of the electron is independent of metal site location. This effect dominates those associated with the metal sites themselves as shown by the fact that the switching potential of **2**$[PF_6]_3$ is only 0.1 more positive than that of **1**$[Cl][PF_6]$.

## Conclusions

Comparison of the switching signal from the $Fe^{III}-Ru^{II}$ cell (**1**[Cl][X]) to that of the $Ru^{III}-Ru^{II}$ cell with larger $d_1/d_m$ (**2**$[PF_6]_3$) shows that the dipolar switching field can be increased by increasing the length of the conjugated linker between the metal sites. This suggests that molecular design can be used to tailor intercell field strengths to accommodate the ancillary ligands of the mixed-valence complexes, ligands that are not present in the quantum dot version of QCA.[6] Counterion properties dominate switching potential magnitudes, and differences between, for example, symmetrical versus unsymmetrical mixed-valence complexes are hidden. Not only do nearby ions strongly affect charge motion within molecules but also through molecules. Indeed, recent experiments demonstrate that the charge state of an ion adjacent to a surface attached molecule strongly perturbs current flow through the molecule to a STM tip.[26]

One important property of the counterion is size, the larger is the size, the smaller is the electrostatic perturbation on the switching potential. Although the counterions constitute a large perturbation on molecular QCA cell switching potential, the results support the use of molecules as charge containers in the QCA paradigm for molecular electronics. The next major question to solve is whether the switching properties of individual mixed-valence complexes are uniform or whether the broad switching peaks observed in this work are derived from a distribution of switching potentials caused by a distribution of counterion locations.

(26) Piva, P. G.; DiLabio, G. A.; Pitters, J. L.; Zikovsky, J.; Rezeq, M.; Dogel, S.; Hofer, W. A.; Wolkow, R. A. *Nature* **2005**, *435*, 658.

## Experimental Section

**General.** Syntheses were carried out under dry argon using standard Schlenk techniques. All procedures were carried out in the dark by wrapping the flasks with aluminum foil. All solvents were distilled prior to use. *cis*-$RuCl_2(dppe)_2$[19] and *trans*-$[Cl(dppe)_2Ru-(C\equiv C)_6-Ru(dppe)_2Cl]$[16] were synthesized according to the literature procedures. $NaPF_6$, DBU, (1,8-diazabicyclo[5.4.0]-undecene-7-ene), $Cu(OAc)_2$, and 3-amino-propionitrile were purchased from Aldrich and were used as received.

IR spectrum was recorded on a Perkin-Elmer Paragon 1000 FT-IR spectrometer, and samples were prepared as KBr pellets. NMR spectra were measured on a Varian 300 and 500 MHz instrument. Mass spectra (FAB+) are recorded on a JEOL JMS-AX505HA mass spectrometer from a matrix of *p*-nitrobenzyl alcohol. Solution cyclic voltammetric measurements were performed on a BAS Epsilon-EC using Pt working electrode, Pt plate counter electrode, and Pt-wire pseudo reference electrode. Tetrabutylammonium hexafluorophosphate ($Bu_4NPF_6$) (0.1 M) was used as the supporting electrolyte.

*trans*-$[Cl(dppe)_2Ru-(C\equiv C)_6-Ru(dppe)_2Cl]$ (50 mg, 0.024 mmol) and $TlPF_6$ (17.5 mg, 0.05 mmol) were stirred in toluene (20 mL) and 3-amino-propionitrile (10 $\mu$L, excess). The reaction mixture was allowed to stir overnight (approximately 12 h) at room temperature. The resultant solution was concentrated under vacuum, dissolved in $CH_2Cl_2$, and filtered through Celite. The filtrate was concentrated under vacuum to give an orange solid, which was washed successively with ether and dried under vacuum (30 mg, 50.9%). 10 mg of this compound was dissolved in minimum volume of $CH_2Cl_2$ to give orange crystals that were used for the X-ray diffraction. **2**$[PF_6]_2$: IR ($cm^{-1}$) 2116.2, 2052, 1954.0 (C≡C), and 835 ($PF_6^-$). $^{31}P$ ($CDCl_3$): 48.6 (s) and −143.8 ppm (m, $PF_6^-$). $^1H$ ($CDCl_3$): 6.74−7.64 (m, 80H, Ph), 2.63−2.76 (brm, 16H, $4XCH_2CH_2P$), 2.38 (t, 4H, $CH_2CH_2NH_2$), 1.80 ((t, 4H, $CH_2CH_2$-$NH_2$). $^{13}C$ ($CDCl_3$): 134.1−128.4 (Ph, Ru−N≡C−$CH_2$), 127.4 (Ru−C≡C), 99.4 (Ru−C≡C), 64.9, 63.2, 59.6, 52.5 (Ru−C≡C−C≡C−C≡C), 37.4 ($CH_2-NH_2$), 30.1 ($PCH_2CH_2P$), 23.4 (Ru−N≡$CCH_2NH_2$). $FAB^+$ (nitrobenzyl matrix) *m*/*z*: 1040.5 $(M^+)^{2+}$.

**Structure Determinations.** A single crystal of compound **2**$[PF_6]_2$ suitable for X-ray diffraction was obtained by slow evaporation of $CH_2Cl_2$ to give orange needle-shaped crystals. Crystals were examined under a light hydrocarbon oil. Structure solution by direct methods in centrosymmetric space group *Pbcn* (No. 60) revealed the non-hydrogen structure. There are large void spaces in the crystal. These voids were analyzed with SQUEEZE (Spek, 2004) and found to total 2790.4 $Å^3$, 20% of the cell volume. In these voids, 426 $e^-$ were found. This electron density was modeled as $CH_2Cl_2$, the solvent of crystallization. Ten molecules of $CH_2Cl_2$ will account for this electron density and will easily fit in the void spaces.

**Quantum Chemical Calculations.** All calculations on $\mathbf{2}^{3+}$ with all phenyl groups replaced with H atoms[27] were performed with the Gaussian 03 software package[28] with optimization of the nuclear geometry and molecular charge configurations under the effect of external electric fields. The calculations are performed with unrestricted Hartree−Fock methods. For C, N, and H, the standard all-electron basis set 6-31G* was used; for the transition metal Ru, the effective core potential (ECP) basis set LANL2DZ[29−31] was used; and for P, which contains valence p orbitals, LANL2DZ basis set augmented with a d polarization function (coefficient = 0.34)[32] was used. Large basis sets and high level calculations are not necessary because of the gross features of molecular charge configuration, and its response to local fields is required. The initial nuclear geometry is derived from the X-ray structure determination.

**Surface Derivatization of the Si Substrate.** A slice of Si (111, B doped, 0.001 ohm cm) wafer polished on a single side was cleaned for 15 min at 70 °C in (40−50):1:1 $H_2O:NH_4OH:H_2O_2$, by volume, for 15 min at 70 °C in (40−50):1:1 $H_2O:HCl:H_2O_2$, by volume, and finally for 2 h at ∼100 °C in 3:1 $H_2SO_4$ (conc):$H_2O_2$ (30%) by volume. (*Warning: The last cleaning solution must be handled with caution; it can detonate unexpectedly.*) The wafer was rinsed thoroughly with flowing DI water between and after each cleaning. To generate an Si−H surface, the oxidized silicon wafer was dried with an inert gas and immersed in 10% HF solution for 2 min. The resulting hydrophobic surface was rinsed with flowing DI water for 30 s and then dried under argon. The silicon wafer with hydride surface was transferred to a Schlenk tube, evacuated, filled with $Cl_2$, and heated to a temperature of 80 °C. After 20 min, the unreacted chlorine was driven out by inert gas and absorbed by sodium iodide solution. (*Warning: HF and $Cl_2$ are extremely corrosive and must be handled with due precautions.*)

**Formation of the Si−2$[PF_6]_2$ Covalent Bond.** A silicon wafer with a freshly prepared chlorinated surface was placed into a ∼1 mM solution of **2**$[PF_6]_2$ in acetonitrile and allowed to react at room temperature for 3 days. The sample was then taken out and washed in acetonitrile to remove physisorbed material. It was then dried in a stream of inert gas.

**X-ray Photoelectron Spectroscopy (XPS).** X-ray photoelectron spectra were obtained on a Kratos XSAM 800 instrument operating with a Mg Kα X-ray source (1253.6 eV). The pressure in the analytical chamber was in the $10^{-8}$ Torr range. The analysis pass energy was set 80 eV for survey scans and high resolution scans. The film samples were analyzed before capacitance measurements. The binding energy scales are referenced to Si 2p (99.3 eV), and spectra were obtained at an approximate takeoff angle of 90° from the surface. Spectra of Ru 3p, N 1s, F 1s, Cl2p, Si 2p (substrate), and B 1s (dopant) as well as survey scans (1153.6−9.6 eV binding energy) were recorded for the sample. Standard sensitivities were used to estimate relative surface concentrations.

**Monolayer Thickness Measurements.** Ellipsometric thickness measurements were carried out on a VASE (J. A. Woollam Co., Inc.) instrument using white light as the light source. The wavelength changed from 2600 to 9000 Å by 100 Å increments. The measured angles were varied from 65° to 75° by 5° increments. A clean Si(100) wafer with an oxide layer was used to calibrate the instrument. A model of $SiO_2$ on Si was used to calculate the film thicknesses.

**Surface Electrochemistry.** Cyclic voltammetric (CV) and DC potential amperometry (DCPA) measurements of the silicon bound complex **2**$[PF_6]_2$ were performed on a BAS Epsilon-EC using a Pt-plate counter electrode and a Pt-wire pseudoreference electrode along with the highly doped silicon working electrode. All electrochemical measurements were done at room temperature under an inert atmosphere in a dedicated drybox. Tetrabutylammonium hexafluorophosphate ($TBAPF_6$, Aldrich) at 0.1 M concentration in $CH_3CN$ was used as the supporting electrolyte.

**Capacitance Measurements.** A silicon wafer containing a covalently bound film of **2**$[PF_6]_2$ was divided into two equal pieces. One piece was measured as was the control. Before measurement, the other was oxidized at 750 mV for 2 s in tetrabutylammonium hexafluorophosphate [TBA][$PF_6$] in $CH_3CN$ at room temperature in a drybox. The oxidized sample was removed and washed by acetonenitrile, and then dried with inert gas. Capacitance measurements on the films were carried out at 1 MHz using a mercury probe (model 802B, Materials Development Corp., Chatsworth, CA). The wafer is held against the two fresh Hg contacts by atmospheric pressure generated by evacuating the probe. The inner small contact has an area of $5 \times 10^{-3}$ $cm^2$ (confirmed by measuring an oxide layer of known thickness). The outer contact has a larger area of 0.22 $cm^2$. Both Hg electrodes form parallel plate capacitors, and the total capacitance of the two is measured in series

(27) Kurnikov, I. V.; Beratan, D. N. *J. Chem. Phys.* **1996**, *105*, 9561.
(28) Pople, J. A.; et al. *Gaussian 03*, revision A.1; Gaussian, Inc.: Pittsburgh, PA, 2003.
(29) Hay, P. J.; Wadt, W. R. *J. Chem. Phys.* **1985**, *82*, 270.
(30) Hay, P. J.; Wadt, W. R. *J. Chem. Phys.* **1985**, *82*, 299.
(31) Wadt, W. R.; Hay, P. J. *J. Chem. Phys.* **1985**, *82*, 284.
(32) Check, C. E.; Faust, T. O.; Bailey, J. M.; Wright, B. J.; Gilbert, T. M.; Sunderlin, L. S. *J. Phys. Chem.* **2001**, *105*, 8111.

through the doped Si substrate. Consequently, the measurement is dominated by the smaller capacitance, that is, the inner dot. The differential capacitance is measured at 1 MHz, and the equipment developed to perform the pulse-counter pulse measurements has been described previously. Suffice it to say that waveform parameters such as pulse width, delay, etc., can be conveniently controlled using the software with an accuracy of about 1 ms. The time average field on the sample in this type of measurement is zero. Multiple positions on the sample are examined for each wafer to confirm reproducibility. Once we appreciated the greater sensitivity of films of **2**$[PF_6]_2$ relative to **1**$[PF_6]$ to environmental contamination, the yield of functional films was better than 90%.

**Acknowledgment.** The aid of Dr. Roger Nassar in the synthesis of **2** and the support of the National Science Foundation (CCF04-03760) are gratefully acknowledged.

**Supporting Information Available:** X-ray crystallographic data (CIF) for **2**$[PF_6]_2$, table of XPS element binding energies, data analysis of the N 1s ionization as a measure of orientation, and complete ref 28. This material is available free of charge via the Internet at http://pubs.acs.org.

JA054508J